DOI: 10.3727/096368910X494623

CT-2237 Accepted 2/24/2010 for publication in "*Cell Transplantation*"

Effects of MRI Contrast Agents on the Stem cell Phenotype

Annelies Crabbe[a], Caroline Vandeputte[b], Tom Dresselaers[c], Angel Ayuso Sacido[d], Jose Manuel Garcia Verdugo[d], Jeroen Eyckmans[e], Frank P. Luyten[e], Koen Van Laere[b], Catherine M Verfaillie[a], Uwe Himmelreich[c]

a: Stem Cell Institute, K.U.Leuven, Leuven, 3000, Belgium

b: Division of Nuclear Medicine, K.U.Leuven, Leuven, 3000, Belgium

c: Biomedical NMR Unit/ MOSAIC, K.U.Leuven, Leuven, 3000, Belgium

d: Centro de Investigación Príncipe Felipe, CIBERNED, Universidad de Valencia, Valencia, 46013, Spain

e: Laboratory for Skeletal development and joint disorders, K.U.Leuven, Leuven, 3000, Belgium

Annelies Crabbe and Caroline Vandeputte contributed equally to this work

The authors claim no conflict of interest.

Running head: Effect of contrast agent on stem cell

Corresponding author:

Annelies Crabbe

Stamcelinstituut Leuven

O&N1 – Herestraat 49, bus 804, 3000 Leuven, Belgium

Telephone: 003216330292 Fax: 003216330294

Annelies.crabbe@med.kuleuven.be

Abstract

The ultimate therapy for ischemic stroke is restoration of blood supply in the ischemic region and regeneration of lost neural cells. This might be achieved by transplanting cells that differentiate into vascular or neuronal cell types, or secrete trophic factors that enhance self-renewal, recruitment, long-term survival and functional integration of endogenous stem/progenitor cells. Experimental stroke models have been developed to determine potential beneficial effect of stem/progenitor cell based therapies. To follow the fate of grafted cells *in vivo*, a number of non-invasive imaging approaches have been developed. Magnetic Resonance Imaging (MRI) is a high resolution, clinically relevant method allowing *in vivo* monitoring of cells labeled with contrast agents. In this study, labeling efficiency of 3 different stem cell populations (mouse Embryonic Stem Cells, rat Multipotent Adult Progenitor Cells and mouse Mesenchymal Stem Cells) with three different (ultra) small superparamagnetic iron oxide (U)SPIOs particles (Resovist®, Endorem®, Sinerem®) was compared. Labeling efficiency with Resovist® and Endorem® differed significantly between the different stem cells. Labeling with (U)SPIOs in the range that allows detection of cells by *in vivo* MRI, did not affect differentiation of stem cells when labeled with concentrations of particles needed for MRI-based visualization. Finally, we demonstrated that labeled rMAPC could be detected *in vivo* and that labeling did not interfere with their migration. We conclude that successful use of (U)SPIOs for MRI based visualization will require assessment of the optimal (U)SPIO for each individual (stem) cell population to ensure the most sensitive detection without associated toxicity.

Keywords: Stem cells, MRI, stroke, iron oxide particles, (U)SPIO, animal models

Introduction

Neurological disorders such as stroke result in irreversible brain tissue damage for which there is no available curative treatment yet. An increasing number of investigators are exploring cell replacement approaches to treat neurological disorders, by grafting stem/progenitor cells in animal models (6,18,27,29,40,41,43,47,53). Clinically suitable methods are needed to follow the fate of the grafted cells *in vivo* to understand in a temporal manner mechanisms of stem cell survival and functional integration (22).

Due to its noninvasive nature, high contrast in soft tissue and high spatial resolution, Magnetic Resonance Imaging (MRI) is one of the most powerful clinical diagnostic tools available today. For biomedical applications like cell tracking, grafted cells must be visualized against the background of host tissue. Therefore, cells have to be labeled with contrast agents (for review see (7,16,17,30). One can use positive contrast agents used in T1-weighted MRI such as lanthanoide-chelates (12) or Mn-containing compounds (51,52). Alternatively, negative contrast agents, such as superparamagnetic iron oxide (SPIO) (4,7,24,31,37,54), ultra small superparamagnetic iron oxide (USPIO) particles (4,18,24,31) or micron-sized iron oxide particles (39,46) are highly sensitive and have a dominant effect on the T2/ T2* relaxation times, causing negative contrast enhancement in the regions of interest. Multiple attributes of these particles determine the labeling efficacy of the agents, including the size of the iron oxide particles, the charge and the nature of the coating (for review see (17,30)). These physicochemical characteristics not only affect the efficacy of the particles for MRI, but also their stability, biodistribution, metabolism and their clearance from the vascular system (11). The internalization of (U)SPIOs can be enhanced through pretreatment of these particles with transfection agents. The latter are highly charged macromolecules that have been used to transfect DNA into cells via electrostatic interaction resulting in endosome formation (2,4,18,24).

Although labeling of cells has shown to be successful for many applications, very few studies have evaluated its effects on cell function (1,23,42,44). The goal of this study was to determine whether different stem cell populations being considered for the therapy of neurological disorders, including

murine mesenchymal stem cells (mMSC), murine embryonic stem cells (mESC) and rat multipotent adult progenitor cells (rMAPC) could be labeled with similar efficiency using different nanoparticles. The stability of the labeling after prolonged culture *in vitro* was also evaluated. In addition, potential toxic effects of the labeling on the three stem cell populations were examined. Finally, the possibility of *in vivo* detection of labeled rMAPC was assessed, as well as the effect of the labeling on cell distribution when grafted in the setting of photothrombotic lesions.

Materials & Methods

Cell populations

mMSC from C57Bl/6 mice were obtained from Dr. D Prockop, Tulane University, USA, where they were isolated and shown to differentiate into adipocytes and osteoblasts (33). Isolation and characteristics of rMAPC from Fisher rats has been described elsewhere (5). mESC from 129 mice (R1 line) were received from the Vesalius Research Institute (K.U. Leuven, Belgium). All cell lines were maintained as described previously (48). Prior to use in our studies, mESC were replated feeder-free on 0.1% gelatin (Chemicon, Billerica, USA) coated plates.

Cell labeling

The following magnetic resonance iron-based contrast agents were used: Resovist® (particle diameter 60nm), (Shering, Munchen, Germany), Sinerem® (particle diameter 20-40nm) and Endorem® (particle diameter 80-150nm) (both Guerbet, Roissy, France). Cell labeling was performed by co-culture of the cells with (U)SPIOs with and without transfection agents (23kDa or 388 kDa Poly-L-lysine) for 4 to 24hrs. The concentration of (U)SPIOs was tested in a range of 20 to 500µg total iron per ml of culture medium. Final concentrations used were Resovist®: 50µg/ml; Endorem®: 348µg/ml; Sinerem®: 500µg/ml.

Iron quantification

Cell pellets of labeled and unlabeled cells were collected 24hrs, 48hrs and 72hrs after labeling and mineralized ‘au bain marie’ prior to Induced Coupled Plasma-Mass Spectroscopy (ICp-MS) (Perkin Elmer, Massachussetts, USA). Values per tube were calculated as follows: total iron content per pellet = µg total iron per liter x (mass mineralized BM/density mineralized BM) x dilution (according to Guerbet protocol).

Dextran staining

Cells were fixed with 10% NBF (60% PBS and 40% formaldehyde (Sigma, St Louis, USA)) for 15 min, washed and incubated for 15min with PBS (Sigma) + 0.1% Triton (Sigma). Next, cells were rinsed and stained with mouse anti-dextran-FITC (1:1000, Stem Cell Technologies, Vancouver, Canada) overnight. The next day, cells were rinsed and staining was detected using fluorescent microscope (AxioImager, Zeiss, Gottingen, Germany).

Cell proliferation

Labeled cells were cultured in their specific expansion medium under standard conditions (48). Cells were counted each day using a nucleocounter. Population doubling time (PDT) was calculated as follows: T x Ln2 / Ln(A/A0), with T = time between two cell counts, A= the number of cells at end, A0= the initial number of cells. We followed the PDT of the labeled cell populations for 7days.

Cell differentiation assays

Differentiation of mMSC to the osteogenic and adipogenic lineage was performed according to standardized methods (13,14,35). Differentiation of rMAPC to the endothelial, neuroectodermal and hepatic lineage was performed as described in (48).

In vitro osteogenic assays: Unlabeled and (U)SPIO labeled mMSC were seeded at 10^4 cells/cm² in 24-well plates. After 2 days in culture, the medium was replaced by osteogenic medium [expansion medium supplemented with 100nM dexamethasone, 10mM beta-glycerophosphate and 50µM ascorbic acid 2-sulfate (Sigma)] for 3 weeks (25). The cells were lysed in 150µl PBS containing 0.05% Triton X 100 (Sigma). Alkaline phosphatase activity was measured using a commercially available kit (Kirkegaard & Perry, Guildford, UK), according to the manufacturer's instructions. DNA content was determined with the Quant-iT™ dsDNA HS Assay (Invitrogen). Parallel samples were processed for RNA extraction at 6 and 14 days. After 3 weeks of treatment with osteogenic medium, calcium deposits were stained with alizarin red. After taking pictures with a Nikon Coolpix 995 camera through an inverted microscope (Telaval 31, Zeiss), alizarin red was extracted as described

129 previously and absorbance was measured at 492nm. Unlabeled bone marrow-derived cells (hBMDCs)
130 were used as positive control.

131 *In vitro adipogenesis:* Unlabeled and (U)SPIO labeled mMSC were seeded in 24 well plates at a cell
132 density of 10^4 cells/cm². Cells were allowed to become confluent in expansion medium. Adipogenic
133 induction medium was then added, consisting of expansion medium supplemented with 1µM
134 dexamethasone, 0.5mM methyl-isobutylxanthine, 10µg/ml insulin, and 100mM indomethacin (all
135 from Sigma). After 72 hrs, the medium was changed to adipogenic maintenance medium (10µg/ml
136 insulin in culture medium) for 24 hrs. Cells were treated 4 times with induction medium. The cells
137 were then maintained in adipogenic maintenance medium for 1 week before fixation. After 21 days
138 cells were washed twice with PBS, fixed with 0.2% glutaraldehyde (Sigma) for 5 min, washed with
139 PBS, rinsed in 60% isopropanol, and covered with oil red O solution (0.1% oil red O [Sigma] in 60%
140 isopropanol). After 10 min, cultures were briefly rinsed in 60% isopropanol, washed thoroughly in
141 distilled water, and counterstained with hematoxylin.

142 Differentiation of MAPC to the endothelial, neuroectodermal and hepatic lineage was performed as
143 described in Ulloa-Montoya et al. (48).

144 Briefly, *for endothelial differentiation*, rMAPC were plated in fibronectin-coated wells. On day 1,
145 medium was switched to a differentiation medium (low glucose DMEM/MCDB-201 (60:40)
146 containing 10ng/ml hVEFG-A (R&D Systems), 1X ITS, 1X LA-BSA, 10^{-8}M dexamethasone, 10^{-4}M
147 ascorbic acid 3-phosphate, 100 units of penicillin, 1,000 units of streptomycin and 55µM 2-
148 mercaptoethanol (Cellgro). RNA samples were collected on day 9 for analysis.

149 *For hepatic differentiation*, rMAPC were plated in matrigel coated wells in low glucose
150 DMEM/MCDB-201 (60:40) containing 2% FBS, 0.25X ITS, 0.5X LA-BSA, $0.1x10^{-6}$M
151 dexamethasone, 10^{-4}M ascorbic acid 3-phosphate, 100 units of penicillin, 1,000 units of streptomycin
152 and 55 µM 2-mercaptoethanol. The following cytokines were added sequentially: 100ng/mL Activin-
153 A and 50ng/mL BMP4; 10ng/ml FGF2 and 25ng/mL FGF8b; and 20ng/m HGF and 10ng/ml
154 Oncostatin-M (all from R&D systems). RNA samples were collected on day 20 for analysis.

For neuroectoderm differentiation, MAPC were plated on gelatin coated T75 flasks in N2B27 medium (DMEM-F12:NeurobasalA medium (Invitrogen) 1:1 supplemented with N2 supplement (1x, R&D) and B27 (1x, Invitrogen), 100 units of penicillin, 1,000 units of streptomycin, 55μM 2-mercaptoethanol and 200nM L-glutamine (Invitrogen). After 2 days medium was changed to NSE medium (Euromed medium (Euroclone) supplemented with N2 supplement (1x, R&D), 200nM L-glutamine (Invitrogen), 100 units of penicillin, 1,000 units of streptomycin and bFGF (10ng/ml, R&D) and EGF (10ng/ml, R&D). RNA samples were collected on day 6 for analysis.

RT-qPCR

Experiments were conducted as described (48). For rMAPC and mESC, total RNA from undifferentiated and differentiated cells was extracted using the RNAeasy microkit (Qiagen, Valencia, CA). cDNA was generated by reverse transcription using Superscript III ReverseTranscriptase (Invitrogen, Carlsbad, USA). To test the expression of gene(s) of interest a real-time PCR was performed as follows: 40 cycles of a two step PCR (95°C for 15", 60°C for 45") after initial denaturation (95°C for 10') with 2μl of cDNA solution, 2X SYBR Green Universal Mix PCR reaction buffer (Invitrogen). Expression of target genes was normalized to *Gapdh*. Gene expression level represented as Delta CT: Delta CT ($CT_{\text{gene of interest}} - CT_{GAPDH}$). Primers used for amplification:

rOct 4 (f: CTGTAACCGGCGCCAGAA, r: TGCATGGGAGAGCCCAGA);

rSox2 (f:AACCCCAAGATGCACAACTC, r:CCGGGAAGCGTGTACTTATC);

rPax6 (f:GTCCATCTTTGCTTGGGAAA, r:TAGCCAGGTTGCGAAGAACT);

rVimentin (f: AATGCTTCTCTGGCACGTCT,r: GCTCCTGGATCTCTTCATCG);

rEn1 (f: CAGAGACTCAAGGCGGAGTT,r: CCTGTGGCTTTCTTGATCTTG);

rvWF (f: CCCACCGGATGGCTAGGTATT,r: GAGGCGGATCTGTTTGAGGTT);

rFlk1 (f: CCAAGCTCAGCACACAAAAA,r: CCAACCACTCTGGGAACTGT);

rPecam (f: GGACTGGCCCTGTCACGTT,r: TTGTTCATGGTGCCAAAACACT);

rProx1 (f: GGAGATGGCTGAGAACAAGC,r: AGACTTTGACCACCGTGTCC);

r*Afp* (f: ACCTGACAGGGAAGATGGTG,r: GCAGTGGTTGATACCGGAGT);

r*G6P* (f: AACCTGGTAGCCCTGTCTTT,r: GGGCTTTCTCTTCTGTGTCG);

rAlb (f: TCTGCACACTCCCAGACAAG,r: AGTCACCCATCACCGTCTTC);

rTat (f: AACCTCAGCACCAATGTTCC,r: TCTTCAGAGCACCCTGGACT)

r/mGapdh (f: TGCCACTCAGAAGACTGTGG, r: GGATGCAGGGATGATGTTCT);

mOct4 (f: CCAATCAGCTTGGGCTAGAG, r: CCTGGGAAAGGTGTCCTGTA)

For osteogenic and adipogenic differentiation studies, cells and cell pellets obtained in the *in vitro* differentiation experiments were homogenized in a cell lysis buffer from the RNA-extraction kit (Nucleospin, BD Biosciences). RNA extraction was performed according to manufacturer's recommendations. Complementary DNA (cDNA) was obtained by reverse transcription of 1µg of total RNA with Oligo (dT)20 as primer (RevertAid™ H Minus First Strand cDNA Synthesis Kit; Fermentas Life Sciences). To evaluate gene expression, taqman PCR was performed on Corbett 6000 Rotorgene system (Westburg) using the assay-on-demand probes from Applied Biosystems. (Assay numbers: GAPDH: 4352339E ALP: Mm01187117_m1, iBSP: Mm00492555_m1) cDNA obtained from expanded mBMCs before labeling and treatment was used as a reference sample. Gene expression levels are listed as Delta CT: delta CT ($CT_{\text{gene of interest}} - CT_{\text{GAPDH}}$).

Electron microscopy

Cells were fixed with 3.5 % glutaraldehyde (Electron microscopy Science, Hatfield, USA) for 1hr at 37 ºC. Cells were post-fixed with 1% osmiumtetroxide (Sigma), rinsed, dehydrated and embedded in araldite (Durcupan, Sigma). Semithin sections (1.5µm) were cut with a diamond knife and stained lightly with 1% toluidine blue (Panreac, Barcelona, Spain). Semithin sections were re-embedded in an araldite block and detached from the glass slide by repeated freezing (liquid nitrogen) and thawing. The block with semi-thin sections was cut in ultra-thin (0.05µm) sections with a diamond knife, stained with lead citrate and examined under a Tecnai spirit electron microscopy (FEI). Photographic images were taken with a Morada camera (Soft Image System, Munster, Germany). For (U)SPIOs particle quantifications an average of 5 ultra-thin sections corresponding to different locations were analyzed for every time point and the quantification was carried out by three independent scientists.

FACS (fluorescence-activated cell sorting)

FACS staining was performed as described (48). Unlabeled and (U)SPIO labeled cells were collected by trypsinization, washed with PBS (Invitrogen) containing 3% FBS and blocked for 10 min with 5% rat serum (Jackson ImmunoResearch, West Grove, USA) and 10µl anti CD16/CD32 (2.4G2) antibody (BD bioscience). After washing, cells were incubated for 30 min at 4^{o}C in 3% FBS containing conjugated antibodies. Cells were washed once and resuspended in PBS 3% FBS and analyzed by flow cytometry on FACSCanto (BDPharmingen, San Jose USA). Antibodies used to characterize rMAPC were anti-CD44-FITC (OX-49) and antiCD31-PE (TLD-3A12). Mouse IgG2a,κ (G155-178) and mouse IgG1,κ (MOPC-31C) are respectively used as isotype controls. For mMSC anti-CD44-APC (IM7) and anti-ckit-PE (2B8) were used and rat IgG2b,κ (A95-1) was used as isotype control (all antibodies were from BDPharmingen, San Diego, CA).

Cytogenetics

Evaluation of cell ploidy was performed as described (48). Demecolcine (10µg/ml in HBSS - Invitrogen) was added to the media until 50% of the cells were detached. Media was removed and the remaining attached cells were collected following rinsing. Cells were centrifuged at 1000 RPM for 5 min, and the pellet transferred to a conical tube with PBS. 0.0075M KCl was added, pre-warmed to 37°C. After 10min, cells were centrifuged and the pellet mixed with fixative. Cell suspensions were dropped on the slide and allowed to dry. Slides were stained with 1:5 diluted Wright-Giemsa stain (0.4% w/v in MeOH) in Gurr Buffer (Gibco). The number of chromosomes per cell was enumerated for at least 40 cells under a light microscope (Zeiss).

Photothrombotic animal model and cell injections

Animal experiments were approved by the bioethics committee of K.U.Leuven (P06098, Leuven, Belgium). Male and female NOD-SCID/gamma $c^{-/-}$ mice were obtained from the breeding colony in the SPF facility at K.U.Leuven. Male Fisher 344 rats were purchased from Charles River, Wilmington, USA. All animals were housed with access to food and water. For surgery, 3-week-old mice or 8-

week-old rats were anesthetized intraperitoneally with ketamine (Ketamine 1000, 75 mg/kg;CEVA Santé Animale, Libourne, France) and medetomidin (Domitor, 1 mg/kg; Orion Pharma, Espoo, Finland).

Cortical photothrombosis was induced in 8 mice and 8 rats. A vertical incision was made between the right orbit and the external auditory canal. The upper part of the temporalis muscle was cauterized so that the muscle could be displaced. Photoillumination with green light (wave length, 540nm; bandwith, 80nm) was achieved using a Xenon lamp (model L-4887; Hamamatsu Photonics, Hamamatsu City, Japan) with heat-absorbing and green filters. The irradiation at intensity of 0.68W/cm^2 was directed with a 3mm optic fiber, which was placed on the exposed skin above the Midlle Cerebral Artery. Photoillumination was performed for 20min after intravenous injection of the photosensitizer Rose Bengal (20mg/kg, Sigma-Aldrich) in a tail vein. Control experiments were performed without injection of the photosensitizer. No photothrombotic injury was detected in control animals.

Injection of GFP$^+$ MAPC was performed in 8 control mice to establish detectability thresholds and also in 8 rats 2 days after photothrombosis. The head of the animals was positioned in a stereotactic head frame (Stoelting, Wood Dale, IL) for stereotactic injection into the striatum. The skull was exposed by a small midline incision and a hole was drilled into the skull in the appropriate location, using bregma as the reference point. Stereotactic coordinates starting from the dura were as follows: Lateral +0.20cm for left injection, -0.20cm for right injection; Anterior-posterior +0.05cm; depth 3mm to 2mm (mice). Lateral +0.28 cm for left injection, -0.28 cm for right injection; Anterior-posterior 0.11 cm; depth 4mm (rat). Using a 30-gauge Hamilton syringe (VWR International, Haasrode, Belgium), 10,000 or 50,000 labeled cells were injected in mice or 10,000 or 1,000,000 cells were injected in rat at a rate of 0.25µl/min into left or right striatum, respectively. After injection, the needle was left in place for an additional 5min before slowly withdrawn. Anesthesia was reversed with atipamezol (Antisedan, 0.5mg/kg; Orion Pharma), administered intraperitoneally.

In vitro MRI experiments of labeled cells

For the assessment of the *in vitro* visualization of (U)SPIO labeled cells by MRI, phantoms were built using culture dishes (3.5cm diameter) filled with agar (Sigma-Aldrich, 0.8 % in saline). Drill holes (4mm diameter of a defined depth) were filled with cell suspensions of known concentration. After solidification of the cell-agar suspensions, drill holes were closed with additional agar. All MR images were acquired using a Bruker Biospec 9.4 Tesla small animal MR scanner (Bruker Biospin, Ettlingen, Germany; horizontal bore, 20cm) equipped with actively shielded gradients (600mT m^{-1}). A purpose-built radio-frequency solenoid transmit-receive coil with a length of 6cm and an inner diameter of 4cm was used for all phantom experiments. 2D multi-slice-multi-echo (MSME) experiments were acquired for the calculation of T_2-maps (TR=6,000ms and 10 TE increments of 10ms, 256^2 matrix, 156 x 156 µm in plane resolution, 0.8mm slice thickness). T2* maps were acquired similarly to MSME experiments using a gradient echo pulse sequence and 10 TE increments of 4.5ms. Three-dimensional (3D), high-resolution T_2*- weighted MR images were acquired using a gradient echo sequence (FLASH, TR=200 ms, TE=15 ms, flip angle 30°). The field-of-view was 3.8 x 3.8 x 0.75cm. The resolution was usually 74 x 74 x 59µm.

In vivo MRI experiments

MR images from animals were usually acquired within 12hrs after photothrombosis. Subsequent images were acquired within 12hrs after cell engraftment and were repeated for up to 10 days after implantation. MR images were acquired using an actively decoupled linear polarized RF resonator as transmitter (inner diameter 7cm, Bruker Biospin) with respective mouse and rat brain surface coils (Bruker Biospin) as receiver. After acquisition of 2D multislice localizer images, 2D MSME experiments were acquired for the calculation of T_2-maps (TR=6,000ms and 10 TE increments of 10ms, 256^2 matrix, 156 x 156 µm in plane resolution, 0.8mm slice thickness). High resolution 3D FLASH images were acquired for the visualization of labeled cells thereafter resulting in an isotropic spatial resolution of $100\mu m^3$. Other acquisition parameters were TR = 100ms, TE = 12ms, flip angle 30°. Diffusion-weighted MR images (spin echo) were acquired for the first two time points after the

photothrombotic injury for assessment of injury. Acquisition parameters were: TR = 1500ms, TE = 27 ms, B = 1500, in plane isotropic resolution 156µm^2, 1mm slice thickness.

MRI data processing

Images were processed using Paravision 4 (Bruker Biospin) and NIH ImageJ. Relaxation rates (r_2) were determined as mean values of homogeneous sections of the cell loaded areas in the agar phantoms. Values were compared to those of unlabeled cells in the same phantom. Relative quantification was also performed using 3D T2*-weighted MR images. The relative mean signal intensity of the respective drill holes was determined relative to unlabeled cells (SI=100%). Data were expressed as mean ± SD.

Immunohistochemistry

Animals were sacrificed at 1,5 or 3 weeks after injection with an intraperitoneal overdose (300µl/20g) of pentobarbital (Nembutal; CEVA Santé Animale) and transcardially perfused with 4% (w/v) paraformaldehyde (PFA, Sigma) in PBS. Brains were removed and postfixed overnight in 4% PFA. Serial 50μm coronal sections were made with a microtome (Vibratome, St. Louis, MO). Hematoxylin/ eosin staining was performed for all brains to assess injury. GFP staining was performed for visualization of transplanted cells (1:30, Clonetech, CA, USA).

Statistical analysis

For *in vitro* experiments student's paired two-tailed t test was used for comparison of 2 experimental groups. Changes were identified as significant if $p<0.05$. When multiple groups were compared, Bonferroni correction was applied. Data are shown as mean +/- standard deviation.

Results

Labeling efficiency of mMSC, rMAPC and mESC with Resovist®, Sinerem® and Endorem®

In initial experiments, we tested the optimal time for labeling and whether addition of transfection agents was needed for labeling with Resovist®, Sinerem® and Endorem®. Greater amounts of (U)SPIOs were taken up by cells incubated for 24hrs with either Resovist®, Sinerem® and Endorem® compared to incubation for 4hrs (microscopy after Prussian Blue staining). Hence all subsequent studies were done by incubating cells 24hrs. Particle clustering was observed when 23kDa poly-L-lysine (PLL) instead of 388kDa PLL was used as transfection agent together with Resovist®. Hence, all further experiments were performed using 388kDa PLL. Comparison of (U)SPIOs uptake with and without the transfection agent (PLL) showed that Resovist® and Sinerem® were taken up (more efficiently) in the presence of PLL compared with uptake experiments without the transfection agent. However, uptake of Endorem® was not affected by the presence or absence of PLL (data not shown). Optimal labeling was defined as being able to detect the lowest cell density (15 cells/µl) for one of the three stem cell populations by MRI of phantoms containing labeled cells. After testing various (U)SPIO concentrations and incubation times, this was achieved using the following conditions: 50µg/ml Resovist® combined with 0.75µg/ml Poly-L-Lysine (388 kDa), 500µg/ml Sinerem® combined with 0.75µg/ml Poly-L-Lysine (388 kDa), and 348µg/ml Endorem® without transfection agent for 24hrs (data not shown).

The size, amount, density and localization of (U)SPIO inclusions in the cells was evaluated by transmission electron microscopy (TEM). As shown in Table 1, the number of inclusions per rMAPC was significantly higher for Sinerem® compared to Endorem® and Resovist®. The average size of inclusions, representing clustered (U)SPIOs, was significantly higher for Resovist® and Sinerem® when compared to Endorem®. The density of inclusions was significantly higher for Endorem® and Resovist® compared with Sinerem®. The quantity of internalized iron per cell was evaluated by ICP-MS as shown for time points day1, day2 and day3 after labeling for 24hrs (Fig. 1ABC). When different particles were compared within one cell population, higher concentrations of iron were

detected in rMAPC and mMSC labeled with Resovist® (2.51 and 11.58pg/cell respectively) at day 1, while in mESC the highest concentration of iron was found following labeling with Endorem® (4.14pg/cell) at day 1. In general, the most iron was in average detected in mMSC, most likely due to their larger size (surface area measured by TEM: mMSC 363.61+/-267.76µm²; rMAPC 157.81+/-89.93µm² and mESC 114.54+/-61.48µm²).

The quantity of iron per rMAPC decreased significantly at day3 (fold decrease of 3.9 for Resovist®, 5.3 for Endorem® and 4.25 for Sinerem®). In mESC there was significant decrease of iron for Resovist® by day3 (fold decrease 2.1) and for Sinerem® by day2 (fold decrease 1.4). In contrast, no reduction could be observed in mMSC (see Fig. 1). The number of inclusions over time was also evaluated. As expected, in all three stem cell types, the number of inclusions decreased over time (Fig 1DEF).

In vitro evaluation of cell labeling by MRI

Visualization of stem cells by MRI is only successful if the amount of (U)SPIOs taken up is sufficient to alter contrast in MRI. To determine if sufficient particles were present in cells to be visualized by MRI, we made agar phantoms containing different numbers of labeled cells to determine the minimum detectable cell number. To assess the effect of dilution of intracellular (U)SPIOs due to cell proliferation and its influence on cell detectability, phantoms containing cells were scanned 24hrs, 48hrs and 72hrs after labeling. Figure 2 shows 3D T2* weighted MRI as well as T2- and T2*-maps of cell phantoms. Cell densities as low as 5 cells/µl were detectable for cells labeled with Endorem® (mESC, rMAPC, mMSC) or Resovist® (rMAPC, mMSC). Labeling with Sinerem® resulted in less contrast resulting in a detectability limit in the order of 75cells/µl. The MRI contrast strongly depended on the combination of stem cell type and contrast agent. Resovist® was superior over Endorem® for rMAPC and for mMSC labeling. However, labeling of mESC was most efficient using Endorem® compared to Resovist® (Fig. 2A). Moreover, contrast in T2*-weighted MRI was more pronounced in the larger mMSC for all particles compared to mESC and rMAPC. Absolute quantification of cell numbers was not possible due to large magnetic susceptibility effects of the

labeled cells at high densities. Fitting for T2- and T2*-maps was not possible due to signal quench even for the lowest echo times. Counting of erased pixel clusters in 3D T2*-weighted MR images of cell suspensions of low density (as described by Kustermann et al. (24)) did not yield a correlation with cell numbers due to cell clustering.

When cells were cultured for 48hrs in iron free medium prior to MRI, decreased detectability of labeled cells was observed (Fig. 2B). Consistent with experiments immediately after cell labeling (Fig. 2A), sensitivity of MRI detection strongly depended on the combination of stem cell type and (U)SPIO. In line with the results of iron uptake (Fig. 1), Endorem® was more efficient for mESC labeling whereas Resovist® resulted in better detectability of rMAPC and mMSC. The lower proliferation rates of mMSC compared to rMAPC and mESC resulted in less dilution of the contrast agents with time and similar detectability thresholds after additional 72hrs incubation in iron free medium (data not shown).

Effect of labeling on stem cell proliferation, phenotype and genetic integrity

We evaluated whether labeling of mMSC, rMAPC and mESC with either (U)SPIO affects cell proliferation over a period of 7 days. Results are shown in Fig 3. Labeling of mMSC with Sinerem® resulted in an increased PDT on d5, compared with unlabeled cells or cells labeled with Endorem® and Resovist®. However by day 7, no significant differences were noted between mMSC labeled with any of the contrast agents compared with unlabeled mMSC (Fig. 3A). Labeling with any of the contrast agents did not affect mESC PDT over the 7 day period (Fig. 3B). By contrast, labeling of rMAPC with either Sinerem® or Endorem® resulted in a lengthening of the PDT on d5, which was statistically significant compared to cells labeled with Resovist® or unlabeled cells (Fig. 3C). The phenotype of mMSC, rMAPC and mESC was validated following labeling with the different (U)SPIOs. mESC represent pluripotent stem cells (21), characterized by the expression of key transcription factors that maintain the pluripotent state. Among these is the *Pou5f1* transcription factor, also known as *Oct4* (32). We determined the transcript levels of *Oct4* in mESC 2 days after labeling with the (U)SPIOs. In Resovist® labeled mESC, the level of O*ct4* transcripts was 2.77 fold higher compared to control,

388 although this was not statistically significant (Fig. 4A). We have previously shown that, similar to
389 mESC but in contrast to mMSC, rMAPC also express *Oct4*, and that presence of *Oct4* is associated
390 with the significantly broader differentiation potential of rMAPC (48). Therefore, the expression of
391 *Oct4* was also evaluated in rMAPC 2 days after labeling with (U)SPIOs and in unlabeled controls. As
392 for mESC, we could not detect a statistically significant difference in *Oct4* transcript levels in rMAPC
393 labeled with any of the (U)SPIOs compared to unlabeled rMAPC (Fig. 4B).

394 We and others have shown that mMSC, used in the present study, express among others the cell
395 surface anitgen CD44 at high levels, but not c-kit (33,47). rMAPC are $CD44^{dim}/CD31^{+}$ (5,48). To
396 ascertain that labeling with (U)SPIOs did not affect the mMSC and rMAPC cell identity, we evaluated
397 cells 3 days after labeling with the 3 contrast agents by FACS. No obvious changes in cell surface
398 phenotype were identified following labeling (Fig 4CD).

399 We also assessed whether labeling with any of the (U)SPIOs would cause increased aneuploidy of
400 mMSC, rMAPC or mESC. It should be noted that previous published studies have shown that mMSC
401 become aneuploid very quickly after isolation, including the mMSC population used here (19).
402 Compared to unlabeled control cells, the ploidy of labeled cells was not decreased for up to five days
403 after labeling (rMAPC: 72.17% +/- 3.50; mESC: 50.9% +/- 8.82; mMSC: 3.3% +/- 0.01).

404 *Effect of labeling on stem cell differentiation*

405 Previous reports suggested that labeling of stem cells, such as mMSC, with (U)SPIOs may affect their
406 differentiation ability (23). We therefore tested the effect of (U)SPIO-labeling on the differentiation
407 ability of mMSC and rMAPC (Fig. 5).

408 mMSC differentiate towards osteoblasts and adipocytes (33,35,36). Treatment with dexamethasone,
409 beta-glycerophosphate and L-ascorbic acid, to induce osteogenic differentiation resulted in a similar
410 increase in alkaline phosphatase (Fig.5A), and calcium deposition by day 14 when labeled and
411 unlabeled mMSC were compared. Statistically significant increases in transcripts for the osteogenic
412 markers, *Alp* (26) and *Bsp* (15), were similar in labeled and unlabeled cells on day 14 of osteogenic

differentiation (Fig. 5B). Adipogenic differentiation was induced using insulin and assessed by Oil Red O staining (Fig. 5C). Cells stained with Oil Red O were similar in labeled or unlabeled cells, for Sinerem®-labeled cells a modest decrease in staining is seen based on visual observations. Hence, labeling of mMSC with Resovist®, Sinerem® or Endorem® did not affect the differentiation ability of mMSC towards osteoblasts and adipocytes. As shown in Fig. 5I-N, TEM demonstrated persistent presence of the different (U)SPIOs in the differentiated mMSC progeny over the whole time period of the experiment.

In comparison with mMSC, rMAPC have significantly broader differentiation ability, and can generate progeny of the three germ layers (48). To assess the effect of (U)SPIO labeling on rMAPC differentiation, differentiation to hepatocyte-, endothelium- and neuroectodermal progenitor-like cells was induced using methods described previously (48). Lineage differentiation was assessed by RT-qPCR for lineage specific gene transcripts (Fig. 5DEF). Differentiation towards hepatocyte-like cells was induced using a multistep protocol as described (48). For labeled or unlabeled cell populations, a similar increase in transcripts for alpha-fetoprotein (*Afp)* (9), albumin *(Alb)* as well as the mature hepatocyte gene *Tat* (8) was seen by day 21 (Fig. 5D). Differentiation to endothelium of rMAPC labeled with (U)SPIOs and unlabeled controls was induced with VEGF-A. A similar induction of *Flk1, Prox1 and Pecam* (20) was observed Fig. 5E. Differentiation of rMAPC towards neuroectodermal progenitor cells was achieved using a protocol based on studies by Conti et al. (10) and described in Ulloa et al. (48). A similar increased expression of transcripts for *Sox2* and *Pax6* (50) was found in labeled and unlabeled cells (Fig. 5F).

Samples from differentiated rMAPC-progeny were fixed and analyzed under TEM. rMAPC-derived hepatocytic and endothelial progeny continued to contain (U)SPIOs in, respectively, 20% and 100% of the cells (Fig. 5GH).

In vivo tracking of labeled cells in the brain

As proof of principle for *in vivo* cell visualization, rMAPC labeled with Resovist® were stereotactically engrafted into the striatum of NOD-SCID γ c $^{-/-}$ mice. 10,000 and 50,000 rMAPC

suspended in 2µl PBS were injected in the left and right hemisphere respectively. Animals were monitored repeatedly by MRI for three weeks. As shown in Fig. 6A-B, 10,000 cells could be visualized in 3D T2* MR images. The contrast and the hypointense volume of the implanted cells in MRI remained constant over the observation period (data not shown). Control injections with PBS or unlabeled cells did not change contrast apart from injuries due to the surgical procedure (needle track). Location of cells in the MRI was confirmed by histology (Fig. 6C).

As also confirmed by MRI, rMAPC were injected 1-3 mm from a photothrombotic lesion. Cells were found along the corpus callosum towards the infarct region within 24hrs. However, no infiltration of rMAPC into the lesion area was seen (Fig. 6D).

Experiments were repeated in eight-week-old Fisher rats with a phototrombotic injury (Fig. 7). Resovist®-labeled rMAPC were injected close to the lesion 24hrs after photothrombosis. Combinations of 100,000 labeled (Resovist®) GFP^+ rMAPC with or without 900,000 unlabeled rMAPC were injected in the brain 2 to 8mm from the photothrombotic injury localized in the cortex of male Fisher rats (n=8). Cell relocation into less dense brain tissue such as the Corpus Callosum and the stroke region or along the needle tract was visualized by MRI (Fig. 7C). Localization of the cells was confirmed with GFP staining and Hematoxylin-eosin staining (Fig. 7DE). Unlabeled control cells showed a similar distribution pattern suggesting that labeling does not appear to affect the redistribution of rMAPC *in vivo* (Fig. 7B and data not shown). When mMSC were implanted, no redistribution of the cells along the corpus callosum was found (Fig. 7A).

Discussion

Non-invasive imaging plays an important role in stem cell research because it allows following an individual animal over time and studying the temporal behavior of endogenous or transplanted stem cells. One of the most clinically relevant imaging modality is MRI, because of its high spacial resolution in comparison with for instance PET, and the possibility to label cells without the need for genetic manipulation that is needed to introduce other markers such as fluorochromes in cells.

For many applications, contrast agents like highly sensitive (U)SPIOs are used for negative contrast enhancement (4,7,18,31,39,46,54). Due to their physicochemical characteristics, label uptake and stability of the particles in cells differs between different types of (U)SPIOs (2,4,18). In addition, some reports have suggested that (U)SPIO labeling may affect certain biological properties of cells (24,28,38,45). However, only limited data exist on the comparison of labeling efficiency and possible toxicity of the particles on different stem/progenitor cell populations. In this study, cell labeling efficiency of three stem cell populations, mMSC, rMAPC and mESC with three (U)SPIOs (Resovist®, Endorem® and Sinerem®) was compared, and potential adverse effects of different labeling procedures on the biology of the cells was examined.

Two of the three particles tested, Resovist® and Sinerem®, are taken up better by the stem/progenitor cells when PLL 388kDa is added, whereas uptake of Endorem® is not further enhanced when a transfection agent is added to the particle. Our study also demonstrates that different amounts of iron in the culture medium are necessary for the three (U)SPIO to visualize the cells by MRI. Also, the labeling efficiency with three different (U)SPIOs varies significantly when different stem cell populations are compared. This was shown by a combination of techniques, including dextran staining (for Endorem® and Sinerem®), measurement of intra-cellular iron by ICP-MS, electronmicroscopy which also demonstrated that the number and distribution of iron particle inclusions within cells differed for the various (U)SPIOs . These findings were also confirmed by *in vitro* MRI, which reflected the data from ICP-MS. Comparison of electron microscopy with iron quantification (ICP-MS) and MRI indicates that the size and density of occlusions but not the number of occlusions

correlates with the internalized amount of iron and MRI contrast. The small size of Sinerem® results in a larger number of small inclusions that are less dense and therefore contain less iron compared to Endorem® and Resovist®. These results demonstrate that labeling methods will likely need to be optimized for every cell type that is used. Over time, we saw a decrease of iron in the cells. This is mainly due to dilution of (U)SPIOs with cell division but might also occur due to exocytosis of the particles (24). The PDT of mESC and rMAPC is 12hrs, whereas the PDT for mMSC is 48hrs, which explains the significant reduction of iron in rMAPC. However, as this is not observed in mESC, further studies on exocytosis are needed to evaluate the loss of iron. In this study, two cell populations were from murine origin and one from rat. Whether the species origin plays a role in the efficiency of stem cell labeling is not known. Also not known is the mechanism(s) underlying the differences in labeling efficiency between cell types.

The second major goal of this study was to evaluate whether (U)SPIO labeling affects the biology of cells, as at least some studies suggested that labeling of mMSC affects differentiation potential (24,37). No significant alterations were observed in the cell phenotype of mMSC, rMAPC and mESC following labeling, whereas differentiation ability of mMSC or rMAPC remained unchanged. For rMAPC progeny committed to an endothelial and hepatocytic phenotype, the labeling persisted until final differentiation of these cells, demonstrating that the label does not significantly affect stem cell differentiation. However, neural progeny contained few remaining SPIOs, likely due to extensive proliferation occurring during the generation of NSC-like cells from rMAPC. Hence, no images are shown from this experiment. Similarly, labeling persisted in mMSC differentiated to the adipocyte and osteocyte lineage, without influencing the differentiation process. It should be noted, however, that Sinerem® decreased proliferation of mMSC, and both Sinerem® and Endorem® affected the proliferation of rMAPC, even though prolonged culture (until 7 days) resulted in restoration of the proliferation rate. Large numbers of endosomal inclusions might thus affect the proliferation capacity of mMSC and rMAPC. This may particularly be true for rMAPC as the number of inclusions was significantly higher during the initial days of culture, but decreased substantially when rMAPC were maintained in culture which correlated with a restoration of the proliferation rate. One should also note

that higher concentrations of Sinerem® and Endorem® were neccessary for cell labeling to achieve a similar MRI detectability . Although the ploidy of cells was evaluated, and no effect of cell labeling was found, more detailed genotoxicity studies still need to be performed. As no spectral karyotyping or comparative genomic hybridization was performed, we cannot fully ascertain that labeling with (U)SPIO was not genotoxic. As TEM demonstrated that the (U)SPIOs are located nearly exclusively in the cell cytoplasm, genotoxicity is however unlikely.

Finally, we evaluated for rMAPC whether cells labeled with Resovist®, that was taken up the best in rMAPC and provided the most sensitive labeling in phantoms *in vitro*, can also be monitored by MRI following transplantation *in vivo*. When grafted in either mouse or rat brain, with or without stroke, labeled rMAPC were visualized until 15 days after transplantation. In the absence of brain injury, no clear migration of the particles was observed. When grafted in animals that previously underwent photothrombotic stroke, some migration of cells was seen. However, whether this was spontaneous migration along the less dense brain tissue in the Corpus Callosum or directed migration towards the stroke region is still being examined. That the labeled rMAPC did not migrate into the lesion, may be due to the creation of scar tissue around the photothrombotic ischemic lesion (3). As unlabeled cells showed the same pattern, these studies demonstrate that cell labeling does not affect the ability of stem / progenitor cells to migrate *in vivo*.

In conclusion, our study highlights that it is necessary to evaluate the efficiency of cell labeling for every new cell-contrast agent combination whose fate is being followed *in vivo*. Secondly, the effect on biological behavior of cells should be examined. We here found an effect of labeling on the cell proliferation, but not differentiation, consistent with the fact that other investigators have demonstrated for instance also effects of labeling on the in vivo distribution of MSC (34,37).

Although labeling of stem cells with MRI is promising, there are some limitations. First, more optimal particles are needed, that can be taken up by cells without need for potentially toxic transfection agents such as magnetoliposomes (44). A second problem is the dilution of the particle over time when cells divide. If the grafted cells continue to proliferate, this will lead to loss of signal in the majority of the

graft. This problem is not seen in animal models with BLI, as labeling is due to stable transduction of a plasmid or vector in cells (49).

Acknowledgments

We would like to thank Tine Decuyper[a], Nathalie Feyaerts[a], Sarah Mertens[a] and Manja Muijtjens[a] for excellent technical assistance with cell cultures, cytogenetics and RT-qPCR.

We are thankful to Guerbet, Roissy, France for the generous gift of Sinerem® and Endorem®.

Annelies Crabbe is a research assistant of the Flemish Fund for Scientific Research (FWO Vlaanderen). Caroline Vandeputte is funded by a grant from the Institute for the Promotion of Innovation through Science and Technology in Flanders (IWT Vlaanderen). Angel Ayuso Sacido is supported by RETICS.

We gratefully acknowledge the financial support by the European Commission for EC-FP6 network DiMI (LSHB-CT-2005-512146), EC-FP6-STREP-STROKEMAP, EC-FP7 network ENCITE (2008-201842), IWT (IWT-60838-BRAINSTIM), and the K.U. Leuven Centers of Excellence 'MoSAIC' and 'SCIL'.

We thank Aneta Schaap-Oziemlak for her critical review of the manuscript.

570 **References**

571 1.Arbab, A. S.; Yocum, G. T.; Rad, A. M.; Khakoo, A. Y.; Fellowes, V.; Read, E. J.; Frank, J. A.
572 Labeling of cells with ferumoxides-protamine sulfate complexes does not inhibit function or
573 differentiation capacity of hematopoietic or mesenchymal stem cells. NMR Biomed. 18(8):553-559;
574 2005.

575 2. Arbab, A. S.; Yocum, G. T.; Wilson, L. B.; Parwana, A.; Jordan, E. K.; Kalish, H.; Frank, J. A.
576 Comparison of transfection agents in forming complexes with ferumoxides, cell labeling efficiency,
577 and cellular viability. Mol. Imaging 3(1):24-32; 2004.

578 3. Beck, H.; Semisch, M.; Culmsee, C.; Plesnila, N.; Hatzopoulos, A. K. Egr-1 regulates expression of
579 the glial scar component phosphacan in astrocytes after experimental stroke. Am. J. Pathol. 173(1):77-
580 92; 2008.

581 4. Berger, C.; Rausch M.; Schmidt, P.; Rudin, M. Feasibility and limits of magnetically labeling
582 primary cultured rat T cells with ferumoxides coupled with commonly used transfection agents. Mol.
583 Imaging 5(2):93-104; 2006.

584 5. Breyer, A.; Estharabadi, N.; Oki, M.; Ulloa, F.; Nelson-Holte, M.; Lien, L.; Jiang, Y. Multipotent
585 adult progenitor cell isolation and culture procedures. Exp. Hematol. 34(11):1596-1601; 2006.

586 6. Bulte, J. W.; Douglas, T.; Witwer, B.; Zhang, S. C.; Strable, E.; Lewis, B. K.; Zywicke, H.; Miller,
587 B.; van Gelderen, P.; Moskowitz, B. M.; Duncan, I. D.; Frank, J. A. Magnetodendrimers allow
588 endosomal magnetic labeling and in vivo tracking of stem cells. Nat. Biotechnol. 19(12):1141-1147;
589 2001.

590 7. Bulte, J. W.; Kraitchman, D.L. Iron oxide MR contrast agents for molecular and cellular imaging.
591 NMR Biomed. 17(7):484-499; 2004.

592 8. Chen, Y.; Dong, X. J.; Zhang, G. R.; Shao, J. Z.; Xiang, L. X. In vitro differentiation of mouse bone
593 marrow stromal stem cells into hepatocytes induced by conditioned culture medium of hepatocytes. J.
594 Cell. Biochem. 102(1):52-63; 2007.

595 9. Chiao, E.; Elazar, M.; Xing, Y.; Xiong, A.; Kmet, M.; Millan, M. T.; Glenn, J. S.; Wong, W. H.;
596 Baker, J. Isolation and transcriptional profiling of purified hepatic cells derived from human
597 embryonic stem cells. Stem Cells 26(8):2032-2041; 2008.

598 10. Conti, L.; Pollard, S. M.; Gorba, T.; Reitano, E.; Toselli, M.; Biella, G.; Sun, Y.; Sanzone, S.;
599 Ying, Q. L.; Cattaneo, E.; Smith, A. Niche-independent symmetrical self-renewal of a mammalian
600 tissue stem cell. PLoS Biol. 3(9):e283; 2005.
601 11. Corot, C.; Robert, P.; Idee, J. M.; Port, M. Recent advances in iron oxide nanocrystal technology
602 for medical imaging. Adv. Drug Deliv. Rev. 58(14):1471-1504; 2006.
603 12. Crich, S. G.; Biancone, L.; Cantaluppi, V.; Duo, D.; Esposito, G.; Russo, S.; Camussi, G.; Aime,
604 S. Improved route for the visualization of stem cells labeled with a Gd-/Eu-chelate as dual (MRI and
605 fluorescence) agent. Magn. Reson. Med. 51(5):938-944; 2004.
606 13. De Bari, C.; Dell'Accio, F.; Tylzanowski, P.; Luyten, F. P. Multipotent mesenchymal stem cells
607 from adult human synovial membrane. Arthritis Rheum. 44(8):1928-1942; 2001.
608 14. De Bari, C.; Dell'Accio, F.; Vanlauwe, J.; Eyckmans, J.; Khan, I. M.; Archer, C. W.; Jones, E. A.;
609 McGonagle, D.; Mitsiadis, T. A.; Pitzalis, C.; Luyten, F. P. Mesenchymal multipotency of adult
610 human periosteal cells demonstrated by single-cell lineage analysis. Arthritis Rheum. 54(4):1209-
611 1221; 2006.
612 15. Guillot, P. V.; De Bari, C.; Dell'accio, F.; Kurata, H.; Polak, J.; Fisk, N. M. Comparative
613 osteogenic transcription profiling of various fetal and adult mesenchymal stem cell sources.
614 Differentiation 76(9):946-957; 2008.
615 16. Himmelreich, U.; Dresselaers, T. Cell labeling and tracking for experimental models using
616 Magnetic Resonance Imaging. Methods 48(2):112-124; 2009.
617 17. Himmelreich, U.; Hoehn M. Stem cell labeling for magnetic resonance imaging. Minim. Invasive
618 Ther. Allied Technol. 17(2):132-142;2008.
619 18. Hoehn, M.; Kustermann, E.; Blunk, J.; Wiedermann, D.; Trapp, T.; Wecker, S.; Focking, M.;
620 Arnold, H.; Hescheler, J.; Fleischmann, B. K.; Schwindt, W.; Buhrle, C. Monitoring of implanted stem
621 cell migration in vivo: a highly resolved in vivo magnetic resonance imaging investigation of
622 experimental stroke in rat. Proc. Natl. Acad. Sci. USA 99(25):16267-16272; 2002.
623 19. Izadpanah, R.; Kaushal, D.; Kriedt, C.; Tsien, F.; Patel, B.; Dufour, J.; Bunnell, B. A. Long-term
624 in vitro expansion alters the biology of adult mesenchymal stem cells. Cancer Res. 68(11):4229-4238;
625 2008.

626 20. Kilic, N.; Oliveira-Ferrer, L.; Neshat-Vahid, S.; Irmak, S.; Obst-Pernberg, K.; Wurmbach, J. H.;
627 Loges, S.; Kilic, E.; Weil, J.; Lauke, H.; Tilki, D.; Singer, B. B.; Ergun, S. Lymphatic reprogramming
628 of microvascular endothelial cells by CEA-related cell adhesion molecule-1 via interaction with
629 VEGFR-3 and Prox1. Blood 110(13):4223-4233; 2007.
630 21. Kim, J.; Chu, J.; Shen, X.; Wang, J.; Orkin, S. H. An extended transcriptional network for
631 pluripotency of embryonic stem cells. Cell 132(6):1049-1061; 2009.
632 22. Koenig, S.; Krause, P.; Hosseini, A. S.; Dullin, C.; Rave-Fraenk, M.; Kimmina, S.; Entwistle, A.
633 L.; Hermann, R. M.; Hess, C. F.; Becker, H.; Christiansen, H. Noninvasive imaging of liver
634 repopulation following hepatocyte transplantation. Cell Transplant. 18(1):69-78; 2009.
635 23. Kostura, L.; Kraitchman, D. L.; Mackay, A. M.; Pittenger, M. F.; Bulte, J. W. Feridex labeling of
636 mesenchymal stem cells inhibits chondrogenesis but not adipogenesis or osteogenesis. NMR Biomed.
637 17(7):513-517; 2004.
638 24. Kustermann, E.; Himmelreich, U.; Kandal, K.; Geelen, T.; Ketkar, A.; Wiedermann, D.; Strecker,
639 C.; Esser, J.; Arnhold, S.; Hoehn, M. Efficient stem cell labeling for MRI studies. Contrast Media
640 Mol. Imaging 3(1):27-37; 2008.
641 25. Kuznetsov, S. A.; Mankani, M. H.; Robey, P. G. Effect of serum on human bone marrow stromal
642 cells: ex vivo expansion and in vivo bone formation. Transplantation 70(12):1780-1787; 2000.
643 26. Liu, F.; Akiyama, Y.; Tai, S.; Maruyama, K.; Kawaguchi, Y.; Muramatsu, K.; Yamaguchi, K.
644 Changes in the expression of CD106, osteogenic genes, and transcription factors involved in the
645 osteogenic differentiation of human bone marrow mesenchymal stem cells. J. Bone Miner. Metab.
646 26(4): 312-320; 2008.
647 27. Lopez-Gonzalez, R.; Kunckles, P.; Velasco, I. Transient Recovery in a Rat Model of Familial
648 Amyotrophic Lateral Sclerosis after Transplantation of Motor Neurons Derived From Mouse
649 Embryonic Stem Cells. Cell Transplant. 18(10-11):1171-1181; 2009.
650 28. Mai, X. L.; Ma, Z. L.; Sun, J. H.; Ju, S. H.; Ma, M.; Teng, G. J. Assessments of proliferation
651 capacity and viability of New Zealand rabbit peripheral blood endothelial progenitor cells labeled with
652 superparamagnetic particles. Cell Transplant. 18(2):171-181; 2009.

653 29. Modo, M.; Cash, D.; Mellodew, K.; Williams, S. C.; Fraser, S. E.; Meade, T. J.; Price, J.; Hodges,
654 H. Tracking transplanted stem cell migration using bifunctional, contrast agent-enhanced, magnetic
655 resonance imaging. Neuroimage 17(2):803-811; 2002.
656 30. Modo, M.; Hoehn, M.; Bulte, J. W. Cellular MR imaging. Mol. Imaging 4(3):143-164; 2005.
657 31. Neri, M.; Maderna, C.; Cavazzin, C.; Deidda-Vigoriti, V.; Politi, L. S.; Scotti, G.; Marzola, P.;
658 Sbarbati, A.; Vescovi, A. L.; Gritti, A. Efficient in vitro labeling of human neural precursor cells with
659 superparamagnetic iron oxide particles: relevance for in vivo cell tracking. Stem Cells 26(2):505-516;
660 2008.
661 32. Niwa, H.; Miyazaki, J.; Smith, A. G. Quantitative expression of Oct-3/4 defines differentiation,
662 dedifferentiation or self-renewal of ES cells. Nat. Genet. 24(4):372-376; 2000.
663 33. Peister, A.; Mellad, J. A.; Larson, B. L.; Hall, B. M.; Gibson, L. F.; Prockop, D. J. Adult stem
664 cells from bone marrow (MSCs) isolated from different strains of inbred mice vary in surface epitopes,
665 rates of proliferation, and differentiation potential. Blood 103(5):1662-1668; 2004.

666 34. Pisanic, T. R., II.; Blackwell, J. D.; Shubayev, V. I.; Finones, R. R.; Jin, S. Nanotoxicity of iron
667 oxide nanoparticle internalization in growing neurons. Biomaterials 28:2572-2581; 2007.
668 35. Pittenger, M. F.; Mackay, A. M.; Beck, S. C.; Jaiswal, R. K.; Douglas, R.; Mosca, J. D.; Moorman,
669 M. A.; Simonetti, D. W.; Craig, S.; Marshak, D. R. Multilineage potential of adult human
670 mesenchymal stem cells. Science 284(5411):143-147; 1999.
671 36. Prockop, D. J. Marrow stromal cells as stem cells for nonhematopoietic tissues. Science
672 276(5309):71-74; 1997.
673 37. Schafer, R.; Ayturan, M.; Bantleon, R.; Kehlbach, R.; Siegel, G.; Pintaske, J.; Conrad, S.;
674 Wolburg, H.; Northoff, H.; Wiskirchen, J.; Weissert, R. The use of clinically approved small particles
675 of iron oxide (SPIO) for labeling of mesenchymal stem cells aggravates clinical symptoms in
676 experimental autoimmune encephalomyelitis and influences their in vivo distribution. Cell Transplant.
677 17(8):923-941; 2008.
678 38. Schafer, R.; Kehlbach, R.; Muller, M.; Bantleon, R.; Kluba, T.; Ayturan, M.; Siegel, G.; Wolburg,
679 H.; Northoff, H.; Dietz, K.; Claussen, C. D.; Wiskirchen, J. Labeling of human mesenchymal stromal

680 cells with superparamagnetic iron oxide leads to a decrease in migration capacity and colony
681 formation ability. Cytotherapy 11(1):68-78; 2009
682 39. Shapiro, E. M.; Gonzalez-Perez, O.; Manuel Garcia-Verdugo, J.; Alvarez-Buylla, A.; Koretsky, A.
683 P. Magnetic resonance imaging of the migration of neuronal precursors generated in the adult rodent
684 brain. Neuroimage 32(3):1150-1157; 2006.
685 40. Sheen, V. L; Macklis, J. D. Targeted neocortical cell death in adult mice guides migration and
686 differentiation of transplanted embryonic neurons. J. Neurosci. 15(12):8378-8392; 1995.
687 41. Shihabuddin, L. S.; Hertz, J. A.; Holets, V. R.; Whittemore, S. R. The adult CNS retains the
688 potential to direct region-specific differentiation of a transplanted neuronal precursor cell line. J.
689 Neurosci. 15(10):6666-6678; 1995.
690 42. Siglienti, I.; Bendszus, M.; Kleinschnitz, C.; Stoll, G. Cytokine profile of iron-laden macrophages:
691 implications for cellular magnetic resonance imaging. J. Neuroimmunol. 173(1-2):166-173; 2006.
692 43. Snyder, E. Y.; Deitcher, D. L.; Walsh, C.; Arnold-Aldea, S.; Hartwieg, E. A.; Cepko, C. L.
693 Multipotent neural cell lines can engraft and participate in development of mouse cerebellum. Cell
694 68(1):33-51; 1992.
695 44. Soenen, S. J.; Baert, J.; De Cuyper, M. Optimal conditions for labelling of 3T3 fibroblasts with
696 magnetoliposomes without affecting cellular viability. Chembiochem. 8(17):2067-2077; 2007.
697 45. Stroh, A.; Zimmer, C.; Gutzeit, C.; Jakstadt, M.; Marschinke, F.; Jung, T.; Pilgrimm, H.; Grune, T.
698 Iron oxide particles for molecular magnetic resonance imaging cause transient oxidative stress in rat
699 macrophages. Free Radic. Biol. Med. 36(8):976-984; 2004.
700 46. Sumner, J. P.; Shapiro, E. M.; Maric, D.; Conroy, R.; Koretsky, A. P. In vivo labeling of adult
701 neural progenitors for MRI with micron sized particles of iron oxide: quantification of labeled cell
702 phenotype. Neuroimage 44(3):671-678; 2009.
703 47. Torrente, Y.; Polli E. Mesenchymal stem cell transplantation for neurodegenerative diseases. Cell
704 Transplant. 17(10-11):1103-1113; 2008.
705 48. Ulloa-Montoya, F.; Kidder, B. L.; Pauwelyn, K. A.; Chase, L. G.; Luttun, A.; Crabbe, A.;
706 Geraerts, M.; Sharov, A. A.; Piao, Y.; Ko, M. S.; Hu, W. S.; Verfaillie, C. M. Comparative

transcriptome analysis of embryonic and adult stem cells with extended and limited differentiation capacity. Genome Biol. 8(8):R163; 2007.

49. Waerzeggers, Y.; Klein, M.; Miletic, H.; Himmelreich, U.; Li, H.; Monfared, P.; Herrlinger, U.; Hoehn, M.; Coenen, H. H.; Weller, M.; Winkeler, A.; Jacobs, A. H. Multimodal imaging of neural progenitor cell fate in rodents. Mol. Imaging 7(2):77-91; 2008.

50. Wen, J.; Hu, Q.; Li, M.; Wang, S.; Zhang, L.; Chen, Y.; Li, L. Pax6 directly modulate Sox2 expression in the neural progenitor cells. Neuroreport 19(4):413-417; 2008.

51. Wideroe, M.; Olsen, O.; Pedersen, T. B.; Goa, P. E.; Kavelaars, A.; Heijnen, C.; Skranes, J.; Brubakk, A. M.; Brekken, C. Manganese-enhanced magnetic resonance imaging of hypoxic-ischemic brain injury in the neonatal rat. Neuroimage 45(3):880-890; 2009.

52. Yamada, M; Yang P. In vitro labeling of human embryonic stem cells for magnetic resonance imaging. J. Vis. Exp. 17:827; 2008.

53. Yamashita, T.; Deguchi, K.; Nagotani, S.; Kamiya, T.; Abe, K. Gene and stem cell therapy in ischemic stroke. Cell Transplant. 18(9):999-1002; 2009.

54. Yeh, T. C.; Zhang, W.; Ildstad, S. T.; Ho, C. In vivo dynamic MRI tracking of rat T-cells labeled with superparamagnetic iron-oxide particles. Magn. Reson. Med. 33(2):200-208; 1995.

Tables

Table1: Statistical analysis of number, size and density of inclusions in rMAPC. Cells were fixed and evaluated under TEM; N = number of samples. Density was measured by visual quantification giving number 0 (as control for unlabeled cells) till 5 (big inclusions). Data are presented as mean ± St error; (*) $p < 0.05$.

	Resovist®	**Endorem®**	**Sinerem®**
Number of inclusions	2.93* ±0.53 (n=14)	3.36* ± 0.84 (n=17)	6.35 ± 0.86 (n=20)
Size of inclusions (µm)	1.74* ± 0.23 (n=40)	1.20 ± 0.07 (n=57)	1.46* ± 0.05 (n=127)
Density of inclusions	2.36* ± 0.21 (n=40)	2.56* ± 0.16 (n=57)	1.05 ± 0.02 (n=127)

747 **Figure legends**

748 **Figure 1: Determination of iron content in rMAPC, mESC and mMSC.** (A-C) Iron quantification
749 was performed by ICP-MS. Stem cells were cultured for 24hrs with Resovist®, Endorem® or
750 Sinerem®, washed with PBS twice and cultured for 1, 2 or 3 days without (U)SPIOs before iron
751 quantification. (A) rMAPC, (B) mESC, (C) mMSC (n=3); p< 0.016 (*). (D-F) Number of endosomal
752 inclusions over time determined by TEM. mMSC, rMAPC and mESC were labeled with Resovist®.
753 The amount of inclusions per cell type was measured at time points day1, day3 and day5 after labeling
754 (n=5).

755 **Figure 2: *In vitro* visualization of cells by MRI.** Agar phantoms were filled with 250, 75, 15 and 5
756 rMAPC, mMSC and mESC per microliter, following labeling of the cells with Endorem®, Resovist
757 ®or Sinerem®. (A) 3D T2*-weighted gradient-echo MRI of phantoms loaded with cells labeled for
758 24hrs, followed by 24hrs culture in (U)SPIO free medium. The presence of contrast agent is illustrated
759 by hypointense (dark) contrast. (B) T2-map (left) and T2*-weighted MRI (right) of Endorem® labeled
760 mESC. The phantom was loaded with labeled cells at concentration of 75cells/µl cultured for an
761 additional (1) 1 hr, (2) 24 hrs, (3) 48 hrs, (4) 72 hrs and (5) 120 hrs in Endorem®-free medium.

762 **Figure 3: Population doubling time of rMAPC, mESC and mMSC labeled with different**
763 **(U)SPIOs.** Population doubling time (PDT = T x Ln2 / Ln(A/A0), with T = time between two cell
764 counts, A= the number of cells at end, A0= the initial number of cells) of cells calculated from day 0
765 till day 7 after (U)SPIO labeling for the following conditions: control, Resovist®, Sinerem®,
766 Endorem®. (A) mMSC, (B) mESC and (C) rMAPC (n=3); p=<0.016 (*).

767 **Figure 4: Comparison of phenotype of labeled and unlabeled stem cells.** mMSC, rMAPC, and
768 mESC were labeled with Endorem®, Resovist®, or Sinerem®. (A-B) Two days after culture in
769 (U)SPIO-free medium, RNA was extracted from rMAPC and mESC and levels of *Oct-4* transcripts
770 were determined by RT-qPCR. Data are shown as Delta Ct (n=3) compared with the house keeping
771 gene Gapdh for (A) mESC and (B) rMAPC. (C-D) Three days after culture in (U)SPIO-free medium,
772 the phenotype of mMSC and rMAPC was evaluated by FACS of cells labeled with antibodies against

773 CD44 and c-kit (mMSC) and CD44 and CD31 (rMAPC) Isotype controls are shown in frame. FACS
774 analysis plot for 1 of 3 representative experiment (C) mMSC; (D) rMAPC.

775 **Figure 5: Differentiation capacity of mMSC and rMAPC labeled with (U)SPIOs in comparison**
776 **to unlabeled cells.** (A-C) mMSC labeled with Endorem®, Resovist®, or Sinerem® were allowed to
777 differentiate towards osteoblasts (A-B) or adipocytes (C). (A) Osteoblast differentiation was induced
778 using osteogenic medium and progeny of labeled and unlabeled cells evaluated by
779 immunohistochemistry for alkaline phosphatase staining at day 6, and calcium measurement at day 14
780 (n=2). (B) Specific transcripts measured by RT-qPCR. Delta Ct-values of *Bsp and Alp* are shown.
781 p=<0.05 (*) (C) To induce adipogenic differentiation, labeled and unlabeled cells were cultured with
782 insulin, and progeny evaluated on day 21 by Oil Red O staining. Left: control, right: adipogenic
783 stimulation. Fat vacuoles are formed in the cells. (D-F) rMAPC labeled with Endorem®, Resovist®, or
784 Sinerem® were allowed to differentiate to hepatocyte- (D), endothelium- (E) and neuroprogenitor-like
785 (F) cells as described in materials and methods. Cells were harvested and on day 21, 9 and 6,
786 respectively, and expression of hepatic, endothelial and neuroprogenitor transcripts evaluated by RT-
787 qPCR (n=9). Delta Ct values are shown. (G-N) Evaluation of iron inclusions in differentiated rMAPC
788 and mMSC by TEM. rMAPC labeled with Endorem®, Resovist®, or Sinerem®, were differentiated
789 towards hepatocyte-like, endothelium-like and neuroprogenitor-like cells. On day 21, 9 and 6
790 respectively, cells were evaluated for presence of iron inclusion using TEM. Labeled mMSC were
791 differentiated towards osteoblasts. On day 14 cells were evaluated for presence of iron inclusions
792 using TEM. (G) rMAPC liver Resovist®, (H) rMAPC liver Endorem®, (I) rMAPC endothelium
793 Resovist®, (J) rMAPC Endothelium Endorem®, (K) rMAPC endothelium Sinerem®, (L) mMSC
794 osteoblast Endorem®, (M) mMSC osteoblast Resovist®, (N) mMSC osteoblast Sinerem®. Iron particles
795 are seen as black cluster or indicated by arrows.

796 **Figure 6: Determination of *in vivo* detectability by MR imaging.** Different concentrations of
797 rMAPC were labeled with Resovist®, suspended in 2µl medium and were injected in the striatum of N
798 OD-SCID $\gamma c^{-/-}$ mice. 3D T2*-weighted MR images are shown for (A) control animal (coronal and
799 corresponding (dotted lines) axial view with (1) 10,000 labeled MAPC, (2) 10,000 unlabeled MAPC,

800 (3) saline injection and (4) 2µl medium + Resovist®) and (B) control animal injected with labeled
801 MAPC (coronal and axial view; (1) left 10,000 cells and (2) right 50,000 cells). (C-D) GFP staining of
802 cells; (C) striatum; (D) Cells engrafting along the Corpus Callosum; CC: Corpus Callosum, Cor:
803 cortex, Str: striatum, ML: midline, SR: stroke region.

804 **Figure 7: *In vivo* tracking of labeled cells in the rat brain.** 100,000 cells were injected in the brain
805 of rats with photothrombotic lesions (left hemisphere) in the contralateral hemisphere (left). The
806 panels show left: a diffusion weighted MRI to illustrate the extend of the lesion (acquired immediately
807 after photothrombosis and 24 hrs before cell engraftment); middle: 3D T2*-weighted MRI acquired 24
808 hrs after cell engraftment (coronal view) and on the right the corresponding axial view. The arrows
809 indicate the injection sites. Images were acquired from (A) an animal with engraftment of 100,000
810 Resovist® labeled mMSC (left and right hemisphere; no migration was observed); (B) an animal with
811 engraftment of 100,000 unlabeled rMAPC (left and right); (C) an animal with engraftment of 100,000
812 Resovist® labeled rMAPC (left and right, Note the migration of cells from the injection site towards
813 the site of photothrombotic injury); (D) GFP staining of tissue slices from animal (C), and (E):
814 hematoxylin-eosin staining of tissue slices from animal (C). (D) and (E): CC: Corpus Callosum, SR:
815 Stroke region, Str: Striatum.

816

Figure 1:

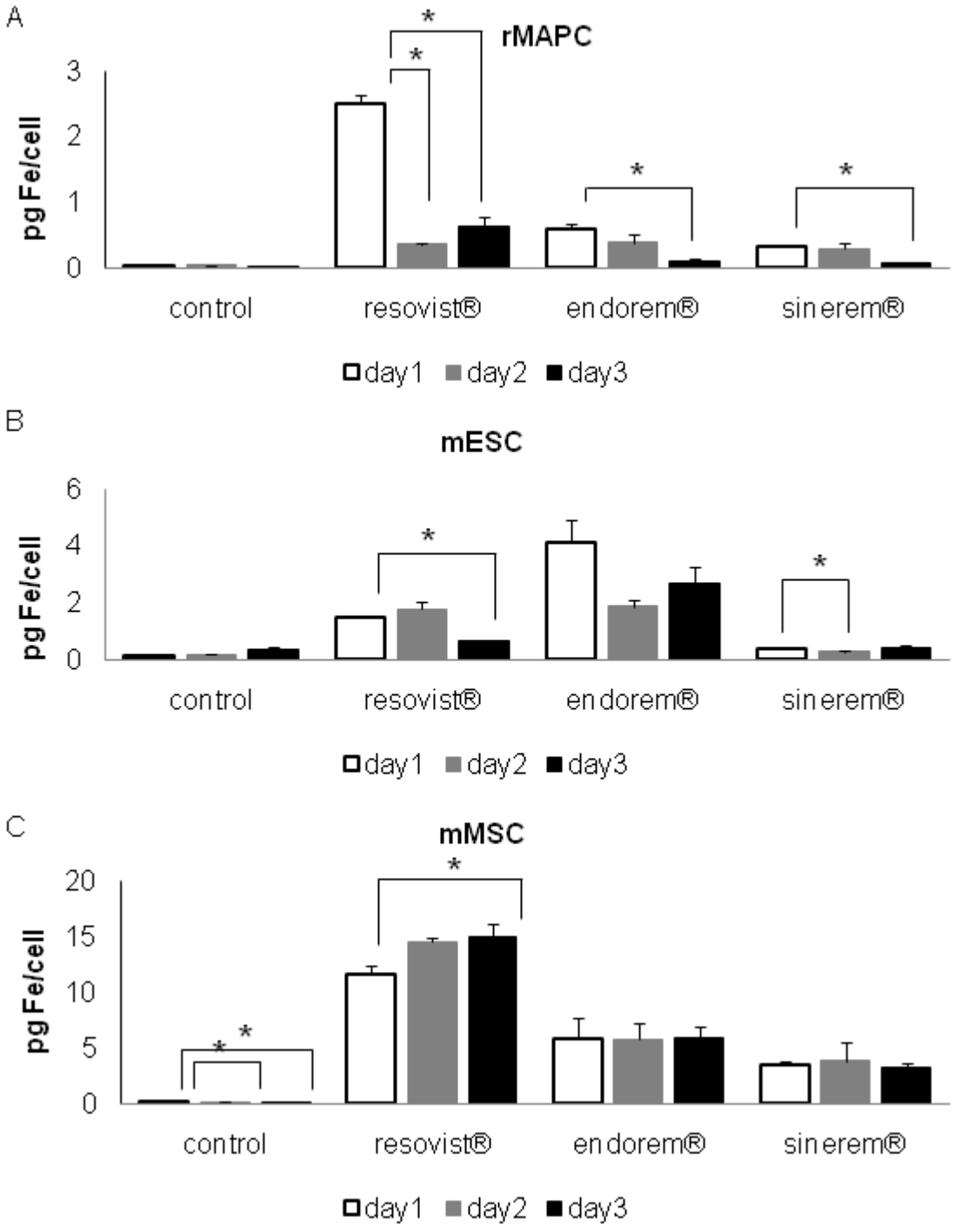
A
rMAPC
pg Fe/cell
3
2
1
0
control
resovist®
endorem®
sinerem®
day1
day2
day3
B
mESC
pg Fe/cell
6
4
2
0
control
resovist®
endorem®
sinerem®
day1
day2
day3
C
mMSC
pg Fe/cell
20
15
10
5
0
control
resovist®
endorem®
sinerem®
day1
day2
day3

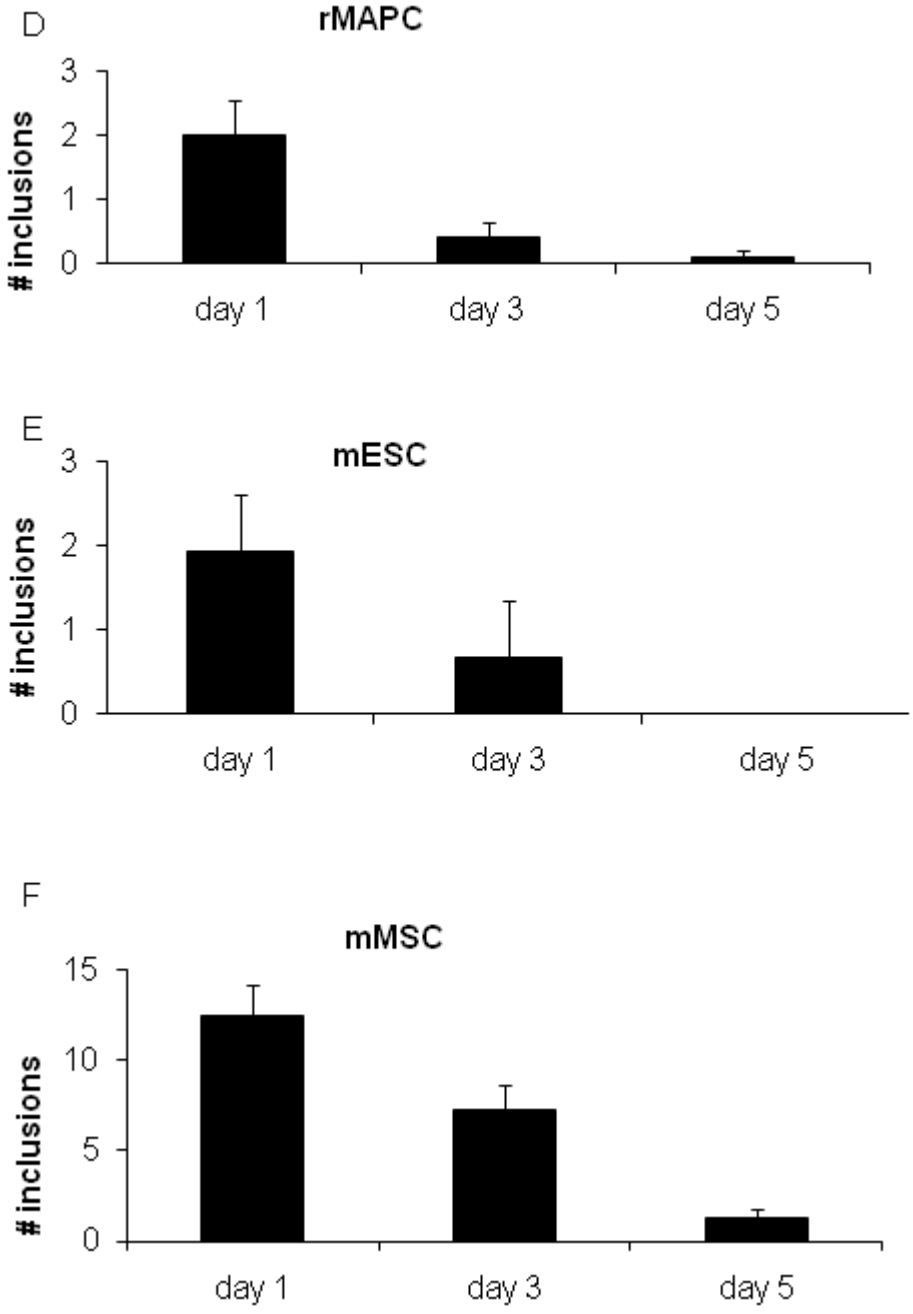
D
rMAPC
inclusions
3
2
1
0
day 1
day 3
day 5
E
mESC
inclusions
3
2
1
0
day 1
day 3
day 5
F
mMSC
inclusions
15
10
5
0
day 1
day 3
day 5

Figure 2:

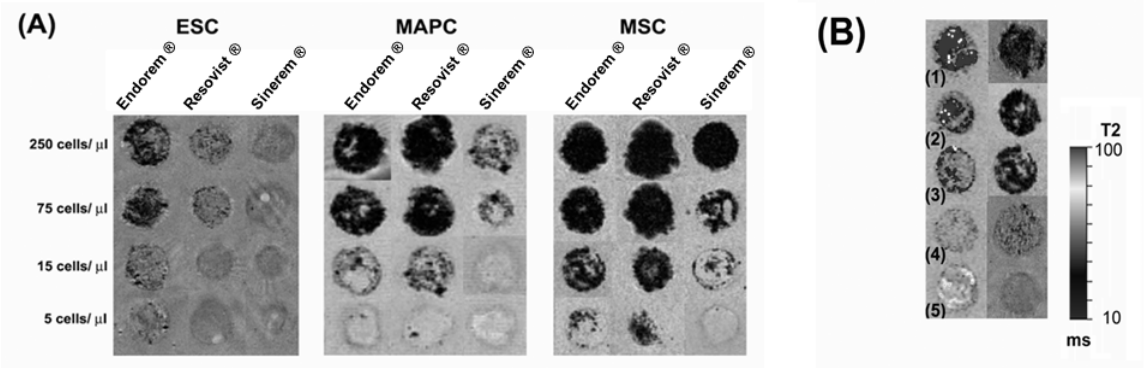
(A)
ESC
MAPC
MSC
Endorem ®
Resovist ®
Sinerem ®
250 cells/ µl
75 cells/ µl
15 cells/ µl
5 cells/ µl
(B)
(1)
(2)
(3)
(4)
(5)
T2
100
10
ms

Figure 3:

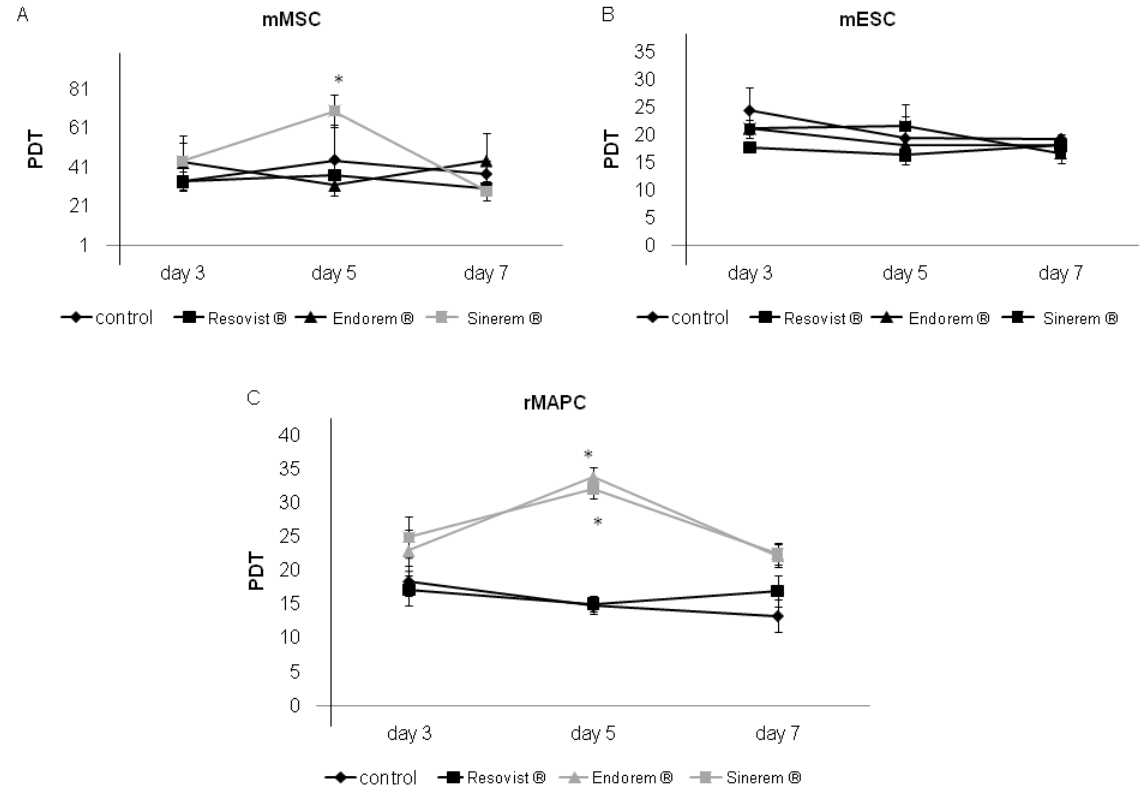
A
mMSC
PDT
81
61
41
21
1
*
day 3
day 5
day 7
control
Resovist ®
Endorem ®
Sinerem ®
B
mESC
PDT
35
30
25
20
15
10
5
0
day 3
day 5
day 7
control
Resovist ®
Endorem ®
Sinerem ®
C
rMAPC
PDT
40
35
30
25
20
15
10
5
0
*
*
day 3
day 5
day 7
control
Resovist ®
Endorem ®
Sinerem ®

Figure 4:

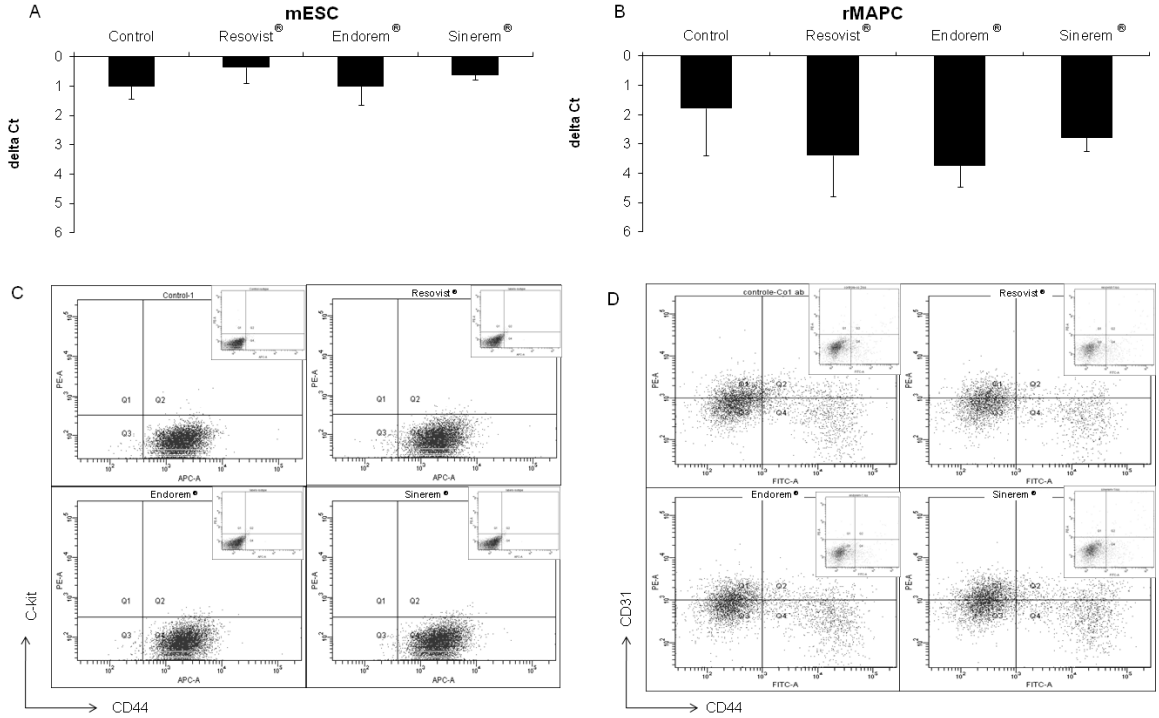
A
mESC
Control
Resovist®
Endorem®
Sinerem®
delta Ct
0
1
2
3
4
5
6
B
rMAPC
Control
Resovist®
Endorem®
Sinerem®
delta Ct
0
1
2
3
4
5
6
C
Control-1
Resovist®
Endorem®
Sinerem®
PE-A
APC-A
Q1
Q2
Q3
Q4
C-kit
CD44
D
controle-Cp1 ab
Resovist®
Endorem®
Sinerem®
PE-A
FITC-A
Q1
Q2
Q4
CD31
CD44

Figure 5:

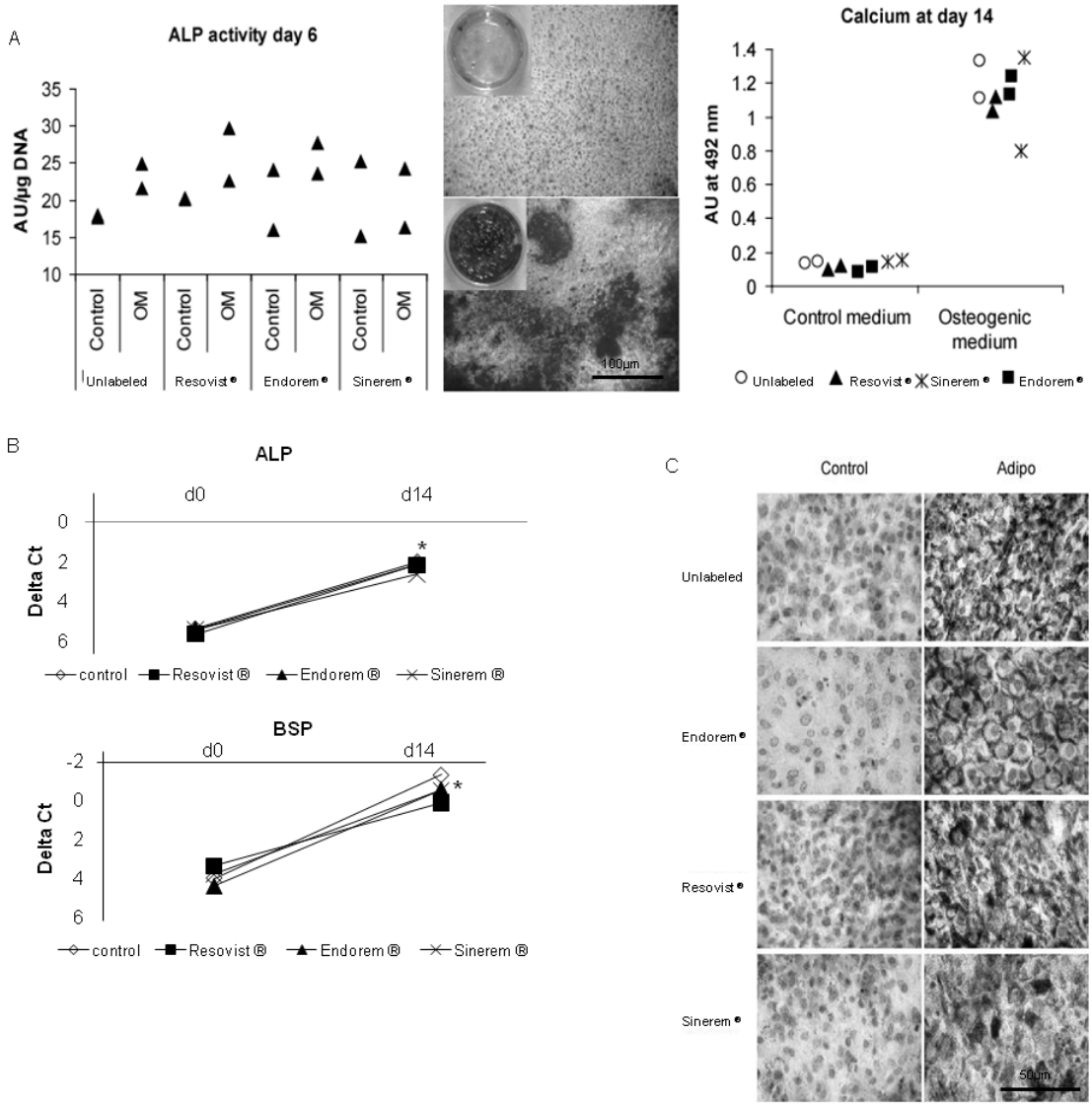
A
ALP activity day 6
AU/µg DNA
35
30
25
20
15
10
Control
OM
Unlabeled
Resovist®
Endorem®
Sinerem®
100µm
Calcium at day 14
AU at 492 nm
1.4
1.2
1
0.8
0.6
0.4
0.2
0
Control medium
Osteogenic medium
Unlabeled
Resovist®
Sinerem®
Endorem®
B
ALP
d0
d14
Delta Ct
0
2
4
6
control
Resovist®
Endorem®
Sinerem®
BSP
-2
C
Control
Adipo
Unlabeled
Endorem®
Resovist®
Sinerem®
50µm

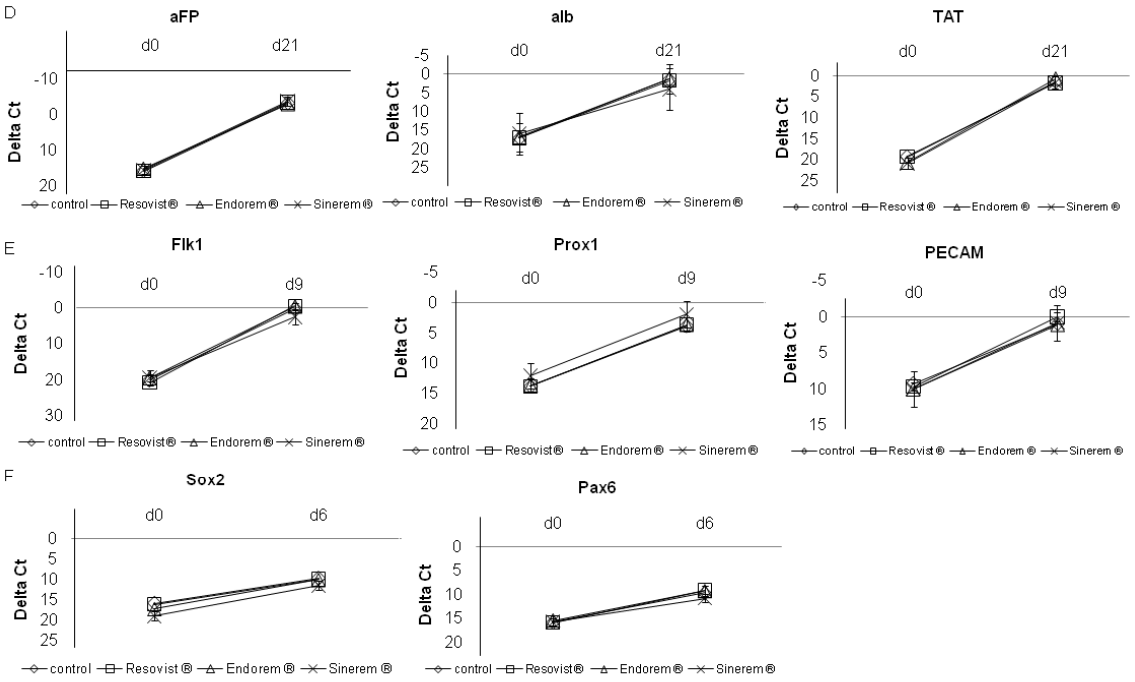
D
aFP
d0
d21
Delta Ct
-10
0
10
20
control
Resovist®
Endorem®
Sinerem®
alb
-5
0
5
10
15
20
25
TAT
E
Flk1
d9
30
Prox1
PECAM
F
Sox2
d6
Pax6

Figure 6:

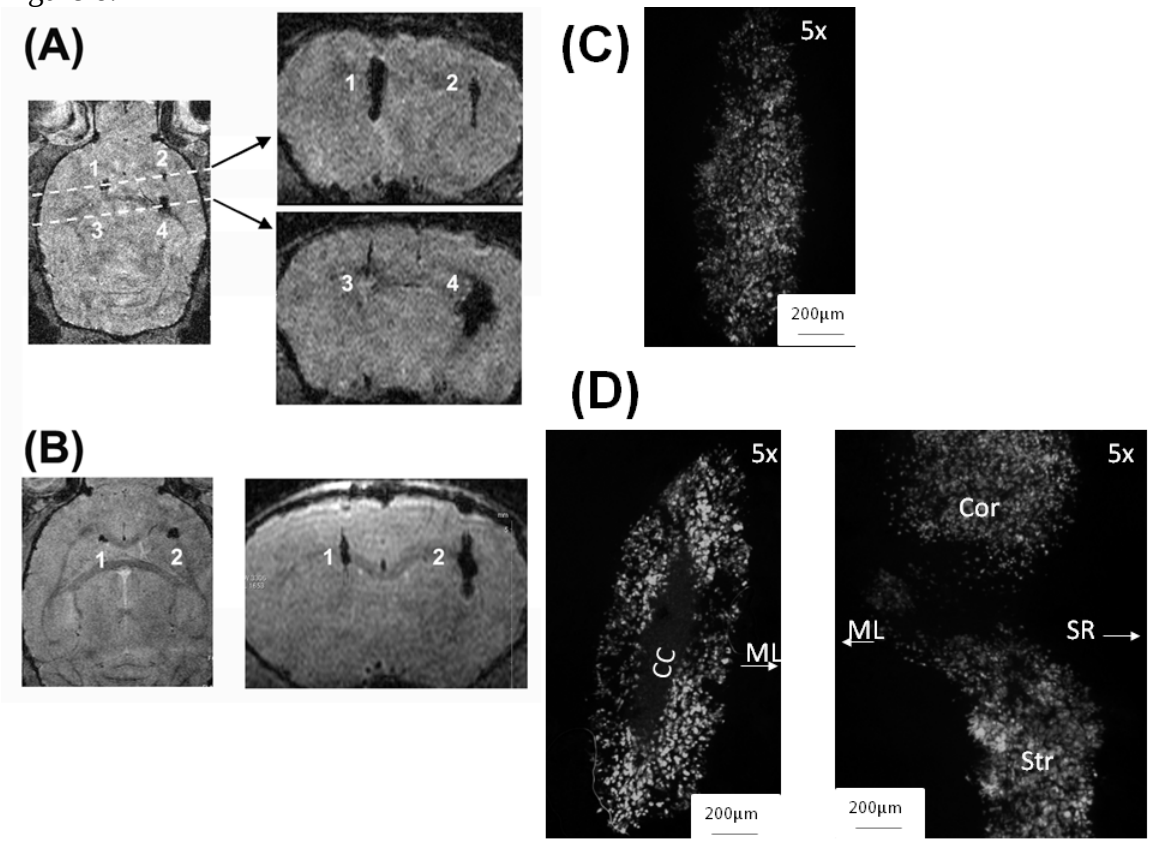
(A)
1
2
3
4
1
2
3
4
(B)
1
2
1
2
(C)
5x
200µm
(D)
5x
CC
ML
200µm
5x
Cor
ML
SR
Str
200µm

Figure 7: